Melt Intercalation in Montmorillonite/Polystyrene Nanocomposites

Nassar, N.; Utracki, L. A.; Kamal, M. R.

Publisher's version / Version de l'éditeur:

International Polymer Processing, pp. 432-431, 2005

*N. Nassar[1], L. A. Utracki[2], M. R. Kamal[1]**

[1] *Chemical Engineering Department, McGill University, Montreal, QC, Canada*
[2] *National Research Council Canada, Industrial Materials Institute, Boucherville, QC, Canada*

Melt Intercalation in Montmorillonite/Polystyrene Nanocomposites

Atactic polystyrene (PS) was used to study the effect of flow field (shear and/or elongational) on the intercalation of polymer/clay nanocomposites (PNC). Three grades of (PS), with different molecular weights, were compounded with an ammonium-modified montmorillonite (Cloisite 10A) in a twin-screw extruder (TSE). The compounds were subsequently fed to a single screw extruder, fitted with one of three specially designed torpedo-attachments. The attachments were designed to provide combinations of different levels of shear and elongational deformations. The resins, TSE compounds, and final PNC's were characterized for the degree of intercalation, degradation, rheological behavior, and mechanical properties. The data showed that the thermal decomposition of the quaternary ammonium intercalant caused severe damage to both PNC components: a collapse of the organoclay interlayer spacing, and the thermo-oxidative degradation of PS. In spite of these detrimental effects, the attachment employing combined elongational and shear flow resulted in generally larger gallery spacing and more improvement of the mechanical properties than the other two attachments.

1 Introduction

Polymer/clay nanocomposites (PNC) exhibit many advantages over conventional composites, while using substantially smaller quantities of filler [1]. For various reasons, it is desirable during nanocomposite manufacturing, to employ processes based on melt exfoliation of modified clay particles. While various researchers have studied the effects of processing variables and material properties on the effectiveness of melt exfoliation [2 to 13], many issues remain unresolved. This study attempts to deal with some of these issues.

Several nanocomposites have been developed to the point of commercial application, and their potential has given rise to large research programs in academic, industrial, and government laboratories [4]. There are many types of nanocomposites. The defining characteristic is simply that the reinforcing phase has at least one dimension in the nanometer range.

* Mail address: Musa R. Kamal, Dept. of Chem. Eng., Wong Bldg., McGill University., 3610 University Street, Montreal, QC, Canada H3A 2B2
E-mail: musal.kamal@mcgill.ca

PNC are emerging as a new class of industrially important materials. At loading levels of 2 to 7 wt.%, they offer similar performance to conventional polymeric composites with 30 to 50 wt.% of reinforcing material. High filler loading in the latter materials causes undesirable increase of density, hence heavy parts, higher melt viscosity, and increased brittleness. Furthermore, the classical composites are opaque with often a poor surface finish. These problems are generally negligible in PNC [1, 4].

PNC have a potential for wide application in the areas of electronics, transportation, construction, packaging, and consumer products [14 to16]. They offer unusual combinations of stiffness and strength that are difficult to attain from individual components [2, 3, 17, 18]. PNC were found to improve flammability resistance [19]. Thermoplastic PNC exhibit substantial reduction of permeability by gases and vapors [20] and the associated solvent uptake rate [18].

The nanoscale structure of the most commonly used PNC is associated with alumino-silicate layers of organically modified smectite silicate, e. g., montmorillonite (MMT). The organoclays usually contain alkyl ammonium or phosphonium cations [21]. The presence of these modifiers in the galleries renders the originally hydrophilic silicate surface organophilic. The meso-structure of nanocomposites depends on the degree of penetration of the polymer into the modified layered silicate framework, producing structures ranging from intercalated to exfoliated.

The greatest combinations of property improvement have been observed for exfoliated PNC [22]. Several techniques have been reported for PNC manufacturing (e. g., in solution, in situ polymerization, or during melt processing). Detailed discussions on this topic may be found in the open and patent literature [1 to 3, 17, 18, 23 to 25]. Several factors are involved in the optimization of PNC manufacturing and properties, such as: properties of the matrix polymer, the molecular architecture of the clay modifier, processing temperature, polymer viscosity, mixing time, shear rate, stress field, etc [26].

Recently, PS/Cloisite® 10A nanocomposites were produced in a twin-screw extruder (TSE) by varying the feed rate (residence time), screw speed and temperature [27]. The data indicated presence of two time-related competitive processes: exfoliation and thermal decomposition of organoclay. The work described in this paper is a continuation of these efforts. The principal goal of this work was to examine the influence of shear and extensional stresses and combined shear and elonga-

tional stress fields on the intercalation/exfoliation of the organoclay. For this purpose, a single screw extruder (SSE) was modified by adding mixing torpedoes with geometries, which engendered the desired flow fields. The evaluated parameters included: clay type, PS molecular weight, residence time, and screw speed. The extent of intercalation/exfoliation in the resulting nanocomposites was evaluated using wide angle X-ray diffraction (WAXD), transmission electron microscopy (TEM), mechanical properties, rheological behavior, and Fourier transform infrared spectroscopy (FTIR).

2 Experimental

2.1 Materials

Three PS resins with different molecular weights were used in this work (PS1510, PS1301, and PS1220). They have melt flow indices 6.5, 3.5, and 1.9 g/10 min, respectively. The resins were manufactured and supplied by NOVA Chemicals (Chesapeake, Virginia). They are generally used in compounding and extrusion applications. The organoclay was Cloisite 10A (C10A) from Southern Clay Products. It is MMT (cation exchange capacity CEC about 0.92 meq/g) intercalated with dimethyl-benzyl-hydrogenated-tallow (2MBHT) quaternary ammonium chloride to CEC = 1.25 meq/g (i. e., ca. 36 % excess).

2.2 Compounding Process

The masterbatches with three grades of PS and containing 10 wt.% of C10A, were diluted with neat resins in a Berstoff co-rotating, intermeshing TSE (Model ZE-25, L/D = 30) to the final composition containing 2 wt.% C10A. The process was carried out at a barrel temperature of 210 °C, screw speed of 200 min^{-1}, and feed rate of 6.3 kg/h. TSE blends were subsequently fed to a SSE (model 1250-20M, L/D = 20), fitted with one of the three specially designed torpedoes. These were designed to provide different combinations of shear and elongational stress fields. Preparation of the masterbatches in TSE, blending the masterbatches with PS in TSE, and extrusion in SSE were carried out without a blanket of nitrogen.

2.3 Attachment Design

Three attachments were used. Since the flow field during melt mixing affects the degree of clay exfoliation, the extruder screw was modified to produce different stress fields. This was accomplished by manufacturing three exchangeable torpedo-type screw attachments for the SSE, and an extension barrel.

The attachments, made from hardened steel, have a basically cylindrical shape with outer diameter, D, identical to that of the screw flights and a length, L = 6D. The front part of the attachments was conical, leaving a uniform 2 mm gap from the inner die surface. The three attachments are described below:

1) Torpedo type S (for smooth) is a smooth cylinder forming 1.10 mm gap inside the barrel extension. The constant annular gap produces pure shear stress to disperse the organoclay agglomerates. This attachment was used to study the effect of shear on the exfoliation/intercalation.
2) Torpedo type G (for grooves) is a cylinder having a transverse radial cross-section that looks like a sinusoidal gear, as can be seen in Fig. 1. The sinusoidal convergent and di-

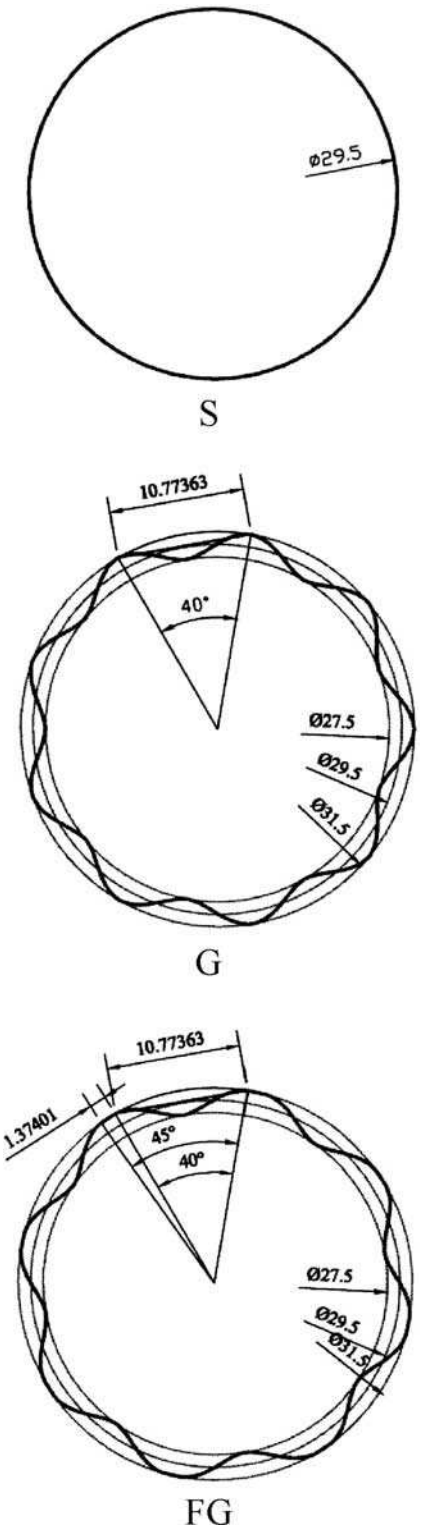

Fig. 1. Attachment cross-sections (all dimensions in mm)

vergent profile, with 1 mm amplitude, leaves 0.1 mm gap with the inner wall of the extended barrel. The converging-diverging flow field generated by this attachment produces significant extensional stresses. Therefore, the purpose of this attachment was to evaluate the influence of elongational flow on the exfoliation/intercalation.

3) Torpedo type FG (for flat grooves) is similar to type G, but the peaks have a 1.3 mm flattop that forms a high shear stress region within the 0.1 mm gap inside the extended barrel. The purpose of this attachment was to generate combined elongation and shear flow.

Fig. 2 provides a 3-dimensional view of the attachments.

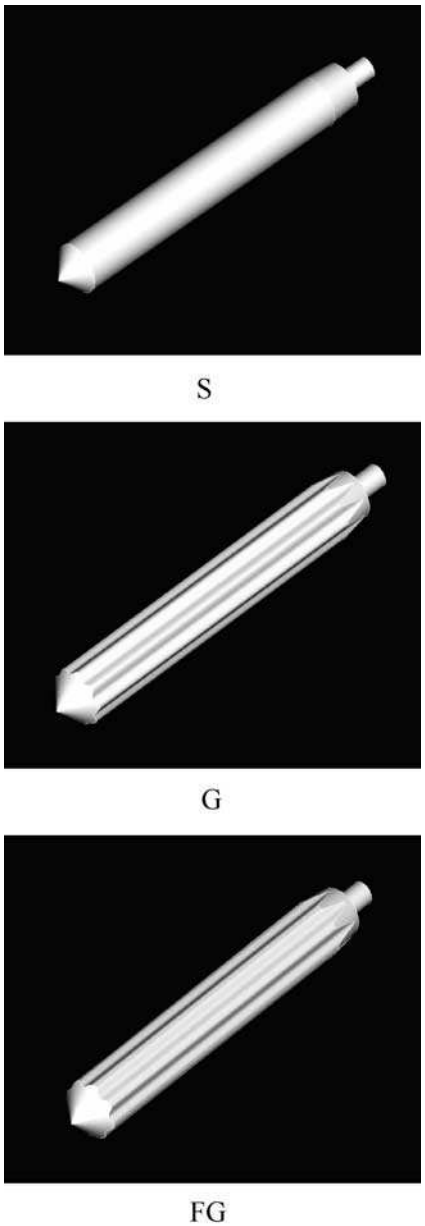

Fig. 2. Attachment geometries (3D)

2.4 Wide-Angle X-ray Diffraction (XRD)

The degree of dispersion and the clay interlayer spacings in the PNC were evaluated using wide angle X-ray diffraction. The spectra were collected using a Rigaku X-ray Inc. $\theta-\theta$ diffractometer. The X-ray source consisted of CuKα radiation with $\lambda = 0.15406$ nm, at a generator voltage of 40 KV and current of 130 mA. The scanning rate was 1^{o}/min in the range 1 to 15°.

2.5 Transmission Electron Microscopy (TEM)

Selected samples were examined by TEM using a TEOL 2000FX with a tungsten (W) filament operating at an accelerating voltage of 80 KV. The TEM was equipped with a wide-angle multi-scan CCD camera (Gatan Bioscan Model 792). The samples were prepared at room temperature using a diamond knife. Care was taken to ensure that the sample thickness was < 100 nm. The samples were collected on grids, which in turn were transferred directly to TEM column.

2.6 Mechanical Testing

Testing was carried out as per ASTM D638, using the Instron Mechanical Tester, model 1123. The specimens were conditioned at the temperature of 23 °C and 60 % humidity. The crosshead speed for all the tests was 500 mm/min. An extensometer was used for determining the deformation. Pneumatic grips were used to prevent slippage. A computer employing Instron Series IX software was used for control and data acquisition.

2.7 Fourier Transform Infrared Spectroscopy Analyses (FTIR)

A Bomem FTIR model 100 apparatus from Bomem-Michelson Inc (Quebec, Canada) was used. Approximately 50 mg thin slices of the PNC specimens (ca. 50 μm) were used. KBr pellets were used in conjunction with C10A organoclay (the ratio of C10A to KBr was 0.01). For the detection of the decomposition products, the cell was placed in the FTIR scanning path and kept at room temperature. The FTIR detection range was 500 to 4000 cm^{-1}.

2.8 Rheology

Dynamic rheological measurements were performed using a Rheometrics Scientific Advanced Rheometrics Expansion System (ARES). Rheological properties of neat PS resins and their nanocomposites were measured using 25 mm diameter parallel plates in the oscillatory shear mode. Dynamic storage modulus, G', and dynamic loss modulus, G'', were recorded as functions of angular frequency, ω at 200 °C. The frequency test range was from 0 to 100 rad/s. Specimens were placed between the preheated parallel plates and were allowed to equilibrate for 15 min prior to each frequency sweep run.

3 Results

3.1 Estimation of Shear/Elongational Stresses Generated by the Torpedoes

For simplicity, a number of assumptions were made: (i) steady state flow, (ii) isothermal flow: constant temperature, (iii) incompressible flow: constant material density, (iv) no slip at the walls: relative velocity of the material is zero at the walls, (v) axial symmetry, and (vi) low R_e: the inertia term is negligible.

In the case of shear stress (torpedo S), there are two stress factors, corresponding to the radial and axial shearing: $\tau_{r\theta}$ and τ_{rz}, respectively. The diameter of the inner cylinder was 31.65 mm, so that the flow channel was 1.1 mm. The shear rate, $\dot{\gamma}$ is given by

$$\dot{\gamma} = \frac{\pi R_1 N_{rev}}{30\delta}, \tag{1}$$

where R_1 is the radius of the wall of the mixer, δ is the gap of the flow channel, and N_{rev} is the RPM of the inner cylinder. Accordingly, the radial stress is:

$$\tau_{r\theta} = \eta\dot{\gamma}, \tag{2}$$

where the viscosity, η, may be determined from the rheological data.

The axial shear stress, τ_{rz}, may be calculated by applying the continuity and momentum equations, therefore:

$$\tau_{rz} = -\frac{\Delta p}{2L}\left(r + \frac{1}{2r}\left(\frac{R_1^2 - R_2^2}{\ln\left(\frac{R_2}{R_1}\right)}\right)\right). \tag{3}$$

It is worth noting that $\Delta p = 0$ (i. e. shear without flow), therefore the axial shear stress $\tau_{rz} = 0$.

The elongational stresses are generated in the wedge-shaped region between the pushing grooves and the barrel (torpedoes G, and FG). The elongation rate in the wedge can be obtained by using a procedure suggested by *Tadmor*, 1968 [28] and further developed by *Rauwendaal* et al. 1999 [29]. The average stretch rate close to the entrance can thus be written as:

$$\dot{\varepsilon} = \frac{(1 + r_d)\,\pi DN\delta \tan\alpha}{H^2}, \tag{4}$$

where α is the wedge angle between the pushing groove and the barrel surface, in our case it is 30°, r_d is the throttle ratio (pressure flow rate divided by drag flow rate), δ is the clearance between the attachment and the barrel, and H is the groove depth. Thus, the elongational stress can be expressed as:

$$\sigma \approx \frac{(1 + r_d)\,\pi DN\delta\eta_e \tan\alpha}{H^2}, \tag{5}$$

where η_e is the elongational viscosity calculated assuming validity of Trouton's rule ($\eta_e = 3\eta$). Table 1 presents elongational and radial shear stresses, for different molecular weight PS, generated by torpedoes S and G. The results are based on 30 min^{-1} and 210 °C. The results show that PS1220 has the highest shear and elongational stresses, as expected. These stresses are expected to counter the attractive forces between the clay platelets.

Attachment	PS	Radial shear (Pa)	Elongational (Pa)
S	PS1510	35 465	–
	PS1301	44 332	–
	PS1220	48 765	–
FG	PS1510	337 962	115 306
	PS1301	422 452	144 131
	PS1220	464 697	158 544

Table 1. Estimation of radial shear and elongational stresses at 30 min^{-1} and 210 °C

3.2 Effect of the Mixing Time

Fig. 3 compares the XRD patterns for neat PS, C10A, and the nanocomposites containing approximately 2 wt.% C10A in PS1220, PS1301, or PS1510. PS1220 was prepared in the SSE with torpedo G, PS1301 with torpedo FG, and PS1510 with torpedo S.

Although PS1301 and PS1510 were extruded using different attachments, the effects of molecular weight and residence time were similar for the two resins. Both show an intercalated shoulder within a short mixing time. Longer mixing did not result in a significant change of the XRD spectra. It has been reported that static intercalation of organoclay by PS takes place in a short time and the equilibrium gallery height is independent of molecular weight of PS, even though the intercalation is slower for higher molecular weight [30]. However, PS1220 (higher molecular weight) did not show a shoulder, which may be due to the high melt viscosity that does not allow the

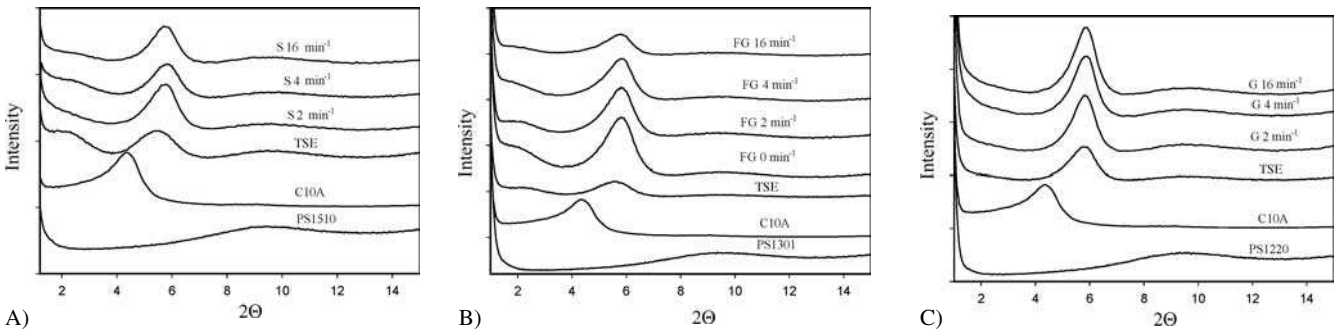

Fig. 3. X-ray patterns for PS and 2 wt.% C10A-containing nanocomposites based on: PS1510 (A), PS1301 (B), PS1220 (C). The screw speed was 30 min-1 and the melt temperature was 210 °C

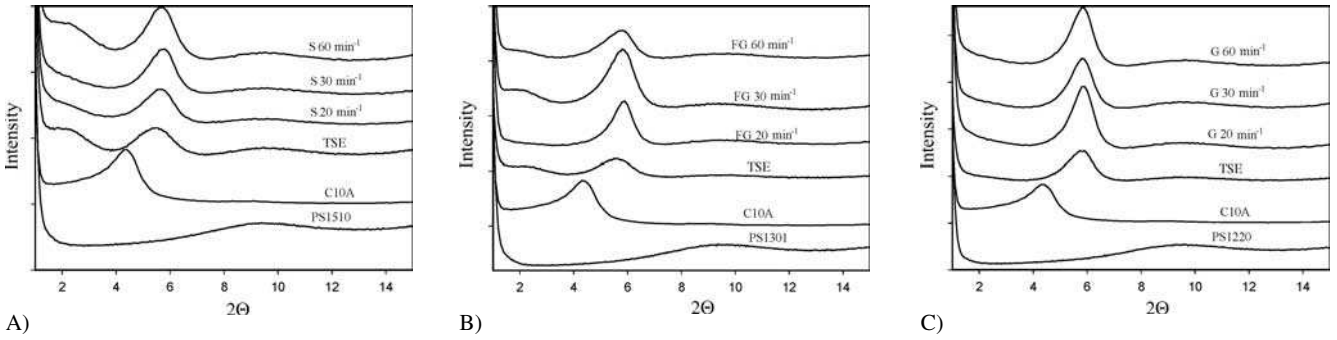

A) B) C)

Fig. 4. X-ray diffraction patterns for PS1510 (A), PS1301 (B) and PS1220 (C) with 2 wt.% C10A at increasing screw speed, with torpedo S, FG, and G, respectively. The residence time was 2 min and the processing temperature was 210 °C

polymer chains to enter into the galleries. Moreover, in all samples, the peak that appears around $2\theta = 6.0^{o}$ (interlayer spacing $d_{001} = 1.5$ nm) suggests a collapsed clay stack structures. This collapse is most likely due to the degradation and/or diffusion of the modifier.

3.3 Effect of Screw Speed

The shear rate during mixing may affect the intercalation of polymer/clay nanocomposites. Fig. 4 shows the effect of screw speed on intercalation of silicate layers by PS.

Again both PS1510 and PS1301 show a shoulder to the left of C10A peak, indicating intercalation, but for PS1220, there is no evidence of a shoulder to the left of the C10A peak. However, in all samples, there are peaks around $2\theta = 6.0^{o}$ (to the right of the C10A peak) corresponding to $d_{001} = 1.5$ nm. Again, this suggests that the organoclay interlayer spacing collapses due to the degradation and/or diffusion of the modifier. It seems that the screw speed does not have a significant effect on the intercalation. *Yoon* et al., 2001 [31] reported that shear applied during mixing accelerates the collapse of interlayer structure of organosilicate and removes the intercalated PS chains out of the gallery. Our results seem to support these observations. However, it should be pointed out that our results with torpedo FG (shear and elongational flow field; see Fig. 4B), indicate improved intercalation. It seems that there is an optimum speed for each combination of attachment and molecular weight. In the case of PS1301 prepared with FG, the intercalation shoulder was most obvious at a speed of $30\ min^{-1}$, while it occurred at $60\ min^{-1}$ for PS1510 with attachment S.

3.4 Effect of Molecular Weight

At the same screw speed, the shear stress increases with molecular weight of PS, due to the higher melt viscosity. Thus, it might be expected that intercalation of organoclay in high molecular weight PS would take place more readily than in low molecular weight PS. However, the results in all figures show the opposite effect. Intercalation seems to be influenced more by diffusion of the polymer chains into the galleries of the silicate clay than by the magnitude of the shear stress applied. Fig. 5 shows the XRD diffraction patterns of PS1510, PS1301, and PS1220 with 2 wt.% C10A compounded in the TSE, prior to dispersion in the modified SSE. The screw speed was $200\ min^{-1}$, and the melt temperature was 210 °C. The TSE extruded PS1510 2 wt.% C10A shows diffraction peaks ($2\theta = 2.4$ and $2\theta = 5.9°$ corresponding to $d_{001} = 3.8$ and 1.5, respectively), indicating the presence of both intercalation and platelet collapse. Similar observations may be made regarding PS1301 2 wt.% C10A. On the other hand, for PS1220 2 wt.% C10A, only collapsed clay structures are present.

3.5 TEM Analysis

To further confirm intercalation of the various PS resins in C10A, TEM studies were carried out (see Fig. 6). The PNCs were prepared in the SSE with different attachments in the melting section, the screw speed was $30\ min^{-1}$, the melt temperature was 210 °C, and the residence time was 2 min. It is obvious that all the samples show collapsed platelets, confirming the XRD analysis results (Figs. 3, 4, and 5). Intercalated tactoids seem to occur in the PS1220 system. On the other hand, PS1301 and PS1510 show intercalated structures and much larger platelet length for PS1220. Again, collapsed clay stacks can be seen.

For the polymer to fully wet and intercalate the clay, the surface polarities of polymer and clay should be matched [32]. Polar interactions are critical for the formation of well-dispersed nanocomposites via melt compounding. It has been shown that the compatibility and optimum interaction between organic modifier, polymer matrix, and silicate layer surface are crucial for the formation of intercalated and especially exfoliated

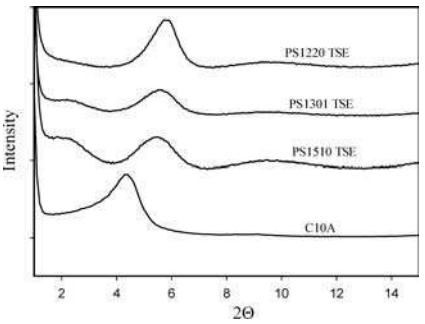

Fig. 5. X-ray diffraction patterns for C10A and C10A nanocomposites based on PS1510, PS1301 and PS1220 matrices containing ca. 2 wt.% C10A

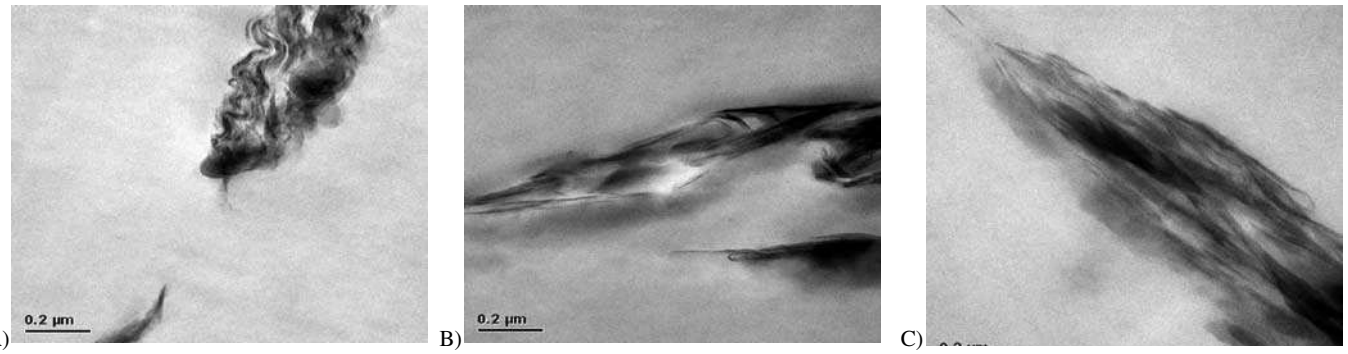

Fig. 6. TEM images for melt processed nanocomposites containing ca. 2 wt.% C10A based on (A) PS1220/G, (B) PS1301/FG and (C) PS1510/S

PNC [31]. Intercalation of PNC might not reach an equilibrium state after completion of the compounding experiment. Since entanglements of polymer chains and arrangement of the clay are not permanent and are altered by flow and relaxation processes, any disturbance, such as shear may disrupt the intercalated platelets and cause collapse [33].

Furthermore, the lack of strong interaction between the ammonium modifier present in C10A and PS chains limits PS intercalation. For these reasons, C10A seems to undergo poor dispersion, with residual large agglomerates. Also, it does not form exfoliated nanocomposites upon mixing with the PS matrix.

3.6 Dynamic Rheology

Fig. 7 shows the rheological behavior at 200 °C of neat PS and composites of PS with C10A based on PS1510. Several trends in Fig. 7A should be noted. Firstly, at low frequency, the PS nanocomposites tend to a plateau beginning at low shear rates. Secondly, the complex viscosities for PS-based nanocomposites are lower than the corresponding neat matrix viscosities. It is noteworthy that the complex viscosities for PS based PNC prepared in TSE are higher than those subsequently prepared in the SSE with torpedo FG. The decrease in viscosities is due to the thermal degradation of modifier as well as the matrix. The degradation effects were observed especially for PNC's with PS1220 as the matrix. In agreement with the observations of *Tanoue* et al., 2004 [27], the effect was related to the number of times that the composition was re-extruded, but not to the total residence time in the extruder. *Cho* and *Paul*, 2001 [34] also observed a lower steady shear viscosity for PA 6 nanocomposites than that of neat polymer, when using a capillary rheometer. The authors suggested that thermal degradation of PA-6 might be a possible mechanism for the lower viscosities. Fig. 7B shows the storage modulus (G') versus the reduced frequency (ω) for PS and PS nanocomposites. For the samples prepared with the TSE, no significant differences can be seen.

Interestingly, the behavior seen for these melt compounded nanocomposites is quite similar to that observed for melt compounded PS nanocomposites, as reported by *Hoffmann* et al., 2000 [35] and Tanoue et al., 2004 [27]. In PS nanocomposites, the PS chains simply diffuse between the platelets and there is no strong interaction between the PS chains and the silicate surface [23]. Thus, in this case, the intercalated nanocomposites do not strongly influence the elastic properties of the PS matrix. However, further processing with the SSE with torpedo FG seems to decrease the G'. This decrease may be due to the thermal degradation of the modifier and/or PS matrix. Similar observations can be made for the loss modulus (Fig. 7C).

3.7 Tensile Test Results

Fig. 8A shows the effect of PS molecular weight and mixing torpedo type on the tensile modulus of nanocomposites melt-mixed with 2 wt.% C10A. The reported tensile modulus is an average of 6 measurements. All changes are within experimental error, except for PS1510. The most significant increases in

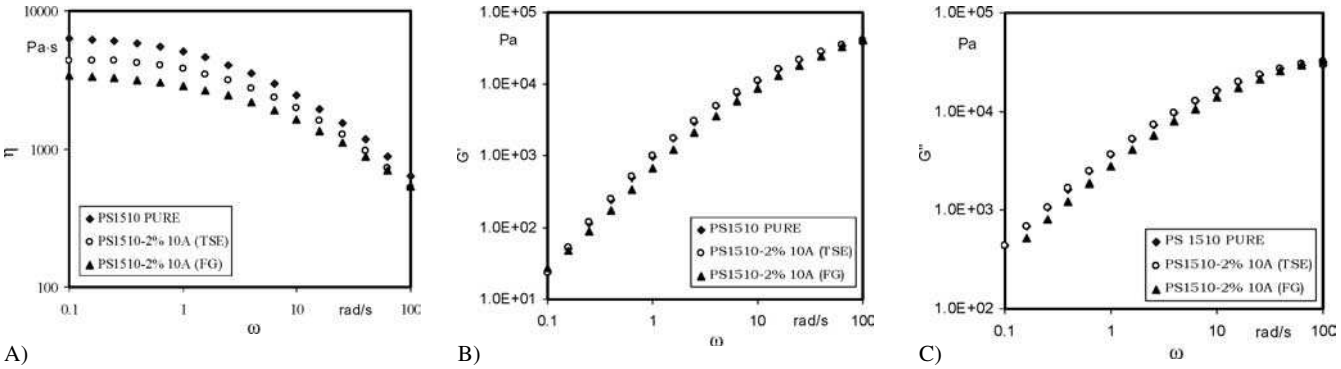

Fig. 7. Dynamic rheological behavior at 200 °C; (A) complex viscosity versus frequency, (B) loss modulus and (C) storage modulus for pure PS1510 and its nanocomposites

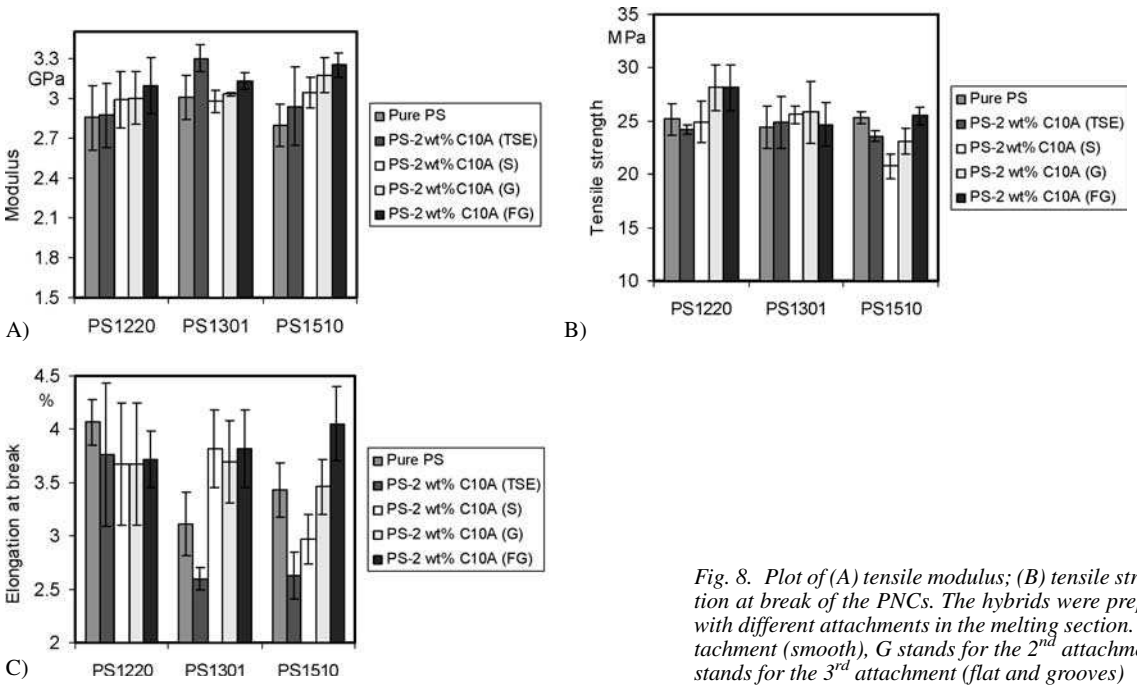

Fig. 8. Plot of (A) tensile modulus; (B) tensile strength and (C) elongation at break of the PNCs. The hybrids were prepared by melt mixing, with different attachments in the melting section. S stands for the 1st attachment (smooth), G stands for the 2nd attachment (grooves), and FG stands for the 3rd attachment (flat and grooves)

tensile modulus are for PS1510. The best performance for this material is with the FG torpedo (15 % modulus increase). These results are consistent with the results obtained with XRD analysis, as shown in Table 2. They indicated that FG generates higher degree of dispersion than G and S. PS1510 and PS1220 appear to show trends of improved modulus by using the torpedoes, in the following order TSE, S, G, FG. The highest modulus for PS1301 is the product of TSE. The slightly larger modulus of PS1301 prepared with TSE may be the result of the additives in this material (lubricants). Further processing with SSE might degrade the lubricants, which leads to decrease in the modulus. PS1510 appears to show a correlation between modulus and d-spacing. As the d_{001} increases, the tensile modulus increases (Fig. 9).

Fig. 8B shows the dependence of tensile strength on clay content and molecular weight. The simplest strength prediction models are based on the area reduction of matrix in the presence of particulate fillers. With the addition of particulate fillers, the strength of plastics generally decreases at lower concentration [36]. However, the tensile strength of the PS resins and the nanocomposites are similar within experimental error in the measurements, and they do not show any consistent systematic pattern. The highest values obtained are for the composites obtained with the high molecular weight material (PS1220) prepared with the G and FG torpedoes.

Torpedo	PS1510		PS1301	
	30 min^{-1}	60 min^{-1}	30 min^{-1}	60 min^{-1}
S	–	4.2	–	4.0
G	3.8	3.4	4.0	3.4
FG	4.0	4.0	4.4	4.0

Table 2. d_{001} spacing for different materials and torpedoes

The relationship between the different matrices and the maximum strain at break for neat PS and PS nanocomposites is displayed in Fig. 8C. The Figure shows that the elongation at break tends to decrease significantly, especially with TSE samples. Further processing with the torpedoes seems to recover some of the lost elongation at break, except for PS1220. The most dramatic effects are observed in PS1510 samples, with torpedoes G and FG yielding the higher values, in that order. At present it is difficult to explain why further processing PS/C10A nanocomposites recovers some of the lost elongation at break. A possible reason is the plasticization effect of the clay modifier.

3.8 FTIR Analysis

FTIR analysis was carried out to assess whether the collapse of the interlayer structure of C10A arises from the thermal degradation of the modifier during melt processing. The organic modifier in the organo-clay starts to decompose rapidly somewhere above 200 °C [37]. Fig. 10 shows the FTIR spectra for C10A after extraction of PS1510 from the hybrids. The peaks

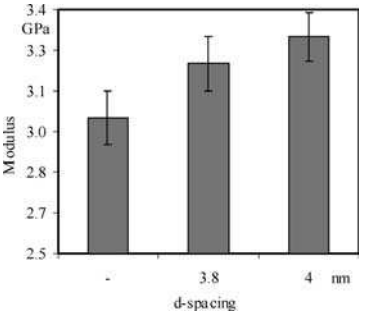

Fig. 9. Correlation between the tensile modulus and d-spacing for PS1510-based nanocomposites

Nomenclature

Δp	pressure drop along the attachment, (Pa)
C10A	Cloisite 10A
d	distance between the parallel plates, (nm)
d_{001}	distance between the parallel plates measured by X-ray (nm)
E	tensile modulus, (Pa)
EXPS	extracted PS
FG	flattop and grooved attachment
FTIR	Fourier transform infrared spectroscopy
G	grooved attachment
G'	storage Modulus, (Pa)
G''	loss Modulus, (Pa)
H	groove depth, (nm)
k	consistency index, (kPa s^n)
MMT	Montmorillonite
n	power law index
N_{rev}	RPM of the inner cylinder, (min^{-1})
PNC	polymer nanocomposites
PS	polystyrene
PS1220	high molecular weight
PS1301	medium molecular weight
PS1510	low molecular weight
R_1	radius of the SSE,(mm)
R_2	radius of the torpedo,(mm)
r_d	throttle ratio (pressure flow rate divided by drag flow rate)
R_e	Reynolds number
S	smooth attachment
SSE	single screw extruder
TEM	transmission electron microscopy
TSE	twin screw extruder
W	Tungsten
XRD	X-ray diffraction

Greek symbols

ω	angular frequency, (rad/s)
σ	elongational stress, (Pa)
τ	shear stress, (Pa)
δ	clearance between the attachment and the barrel, (nm)
λ	wavelength of radiation, (nm)
α	wedge angle between the pushing groove and the barrel surface
η^*	complex viscosity, (Pa s)
η_e	elongational viscosity,(Pa s)
2θ	angle between the diffracted and incoming X-ray waves
η	melt viscosity, (Pa s)
$\dot{\gamma}$	shear rate, (s^{-1})
tan δ	G'/G'' ratio
$\dot{\varepsilon}$	average stretch rate close to the entrance, (s^{-1})

at 1728 and 1264 cm^{-1} are new and correspond to (−COO−) groups formed by oxidation, with the first one corresponding to the carbonyl (C=O) bond and the second to carboxyl (CO−O) bond. The figure shows that the relative intensity of these peaks increases, as the residence time in the extruder increases. These peaks do not appear in the spectra of the neat PS1510 after 16 minutes of heating. Thus, the degradation appears to be related to the modifier.

It is suggested that degradation starts with the Hoffmann elimination reaction of the quaternary amine [27]. The principal effect is the splitting off of the hydrogenated tallow branch with a vinyl group on the end. In the presence of oxygen at the processing temperature, the vinyl readily oxidizes into peroxide, which in turn attacks PS. Thus, extrusion of PS with C10A without nitrogen or antioxidants causes stepwise degradation of organoclay and PS. Since the degradation is oxidative, it occurs every time the PS nanocomposites are heated in an extruder. The samples were oxidatively degraded three times, viz. in the TSE during the preparation of masterbatch, during dilution in the TSE, and in the SSE. It is noteworthy that the clay might act as a catalyst causing the oxidation to a carbonyl species [38]. However, in spite of the degradation, the torpedoes managed to improve the clay intercalation.

4 Discussion and Conclusions

Nanocomposites based on three PS resins, with different molecular weights, were prepared in a co-rotating TSE by compounding with Cloisite 10A (C10A). The compounding was carried out in two steps: preparation of a masterbatch containing 10 wt.% C10A, and subsequent 5-fold dilution. Next, the nanocomposite was exposed to a controlled stress field in a SSE with different attachments in the melt section. During all three extrusions, neither antioxidant nor nitrogen blanket was used. The principal goal of the work was to examine the effect of stress field on the degree of C10A dispersion. The most effective dispersion was achieved with a combined shear and elongational flow field.

X-ray results suggest an intercalated structure in PNC's with PS1510 or PS1301 as the matrix, as shown in Table 2. However, collapse of the organoclay interlayer spacing was observed for all PS-based nanocomposites. TEM revealed generally uniformly distributed clay stacks, intercalated platelets, as well as collapsed platelets. Increasing the residence time or the screw speed in the extruder did not improve significantly

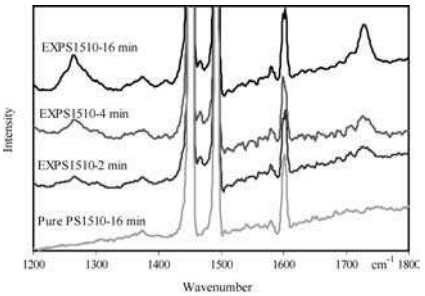

Fig. 10. FTIR spectra of extracted C10A and PS1510. EXPS stands for extracted PS

the dispersion. In the meantime, degradation was found to increase, as the residence time was increased.

In the collapsed peaks, the gallery height of PS/C10A was reduced to below that of C10A. This suggests that the degradation and expulsion of the modifier cause the collapse. FTIR confirmed the intercalant degradation. The degradation starts with Hoffmann decomposition of the quaternary amine. During this process, the quaternary ammonium is decomposed into a volatile amine, and the longest hydrocarbon chain (that of hydrogenated tallow) forms a vinyl end group. The group readily reacts with oxygen to form peroxide, which in turn reacts with the PS matrix, causing chain scission.

The rheological measurements showed that each extrusion resulted in significant decrease of the zero-shear viscosity. As expected, the effect was most severe (ca. 50 %) for the highest molecular weight sample (PS1220), and the lowest (ca. 29 %) was for the lowest molecular weight resin, PS1510. These numbers translate into reduction of the weight-average molecular weight by 18 and 9 %, respectively.

Mechanical properties were consistent with the morphological structure found by XRD and TEM. The tensile strength of the nanocomposites was found to decrease for all molecular weights, while the tensile modulus was found to increase for all the molecular weights. A correlation between tensile modulus and d-spacing was found. Elongation at break decreased significantly, especially for TSE samples, while it recovered some of the lost elongation for the torpedo samples, especially with the low molecular weight resin.

Considering the very severe degradation effects on both PNC components: the organoclay and the PS matrix, expansion of the average interlayer spacing, and the improvements of tensile modulus are particularly noteworthy. Upon incorporation of 2 wt.% of C10A, the relative modulus increased by an amount: $\Delta E = 100[E\,(PNC)/E\,(PS) - 1]$, dependent on the compounding equipment (i. e., TSE or modified SSE) and the PS matrix. Thus, after diluting the masterbatches to 2 wt.% the modulus increased by $\Delta E = 1$, 3, and 5 % for PS1220, PS1310, and PS1510, respectively. However, passing these compositions through the modified SSE (FG attachment), in spite of one additional degradation step, resulted in $\Delta E = 8$, 10, and 16 %, respectively. Since the effects of the two other attachments were negligible, the data show the advantage of the flow field combining elongation and shear.

References

1 *Utracki, L. A.:* Clay-Containing Polymeric Nanocomposites. Rapra, UK (2004)
2 *Kojima, Y., Usuki, A., Kawasumi, M., Okada, A., Kurauchi, T., Kamigaito, O.:* J. Polym. Sci., Part A: Poly. Chem. 31, p. 1755 (1993)
3 *Kojima, Y., Usuki, A., Kojima, Y., Kawasumi, M. Okada, A., Kurauchi, T., Kamigaito, O.:* J. Polym. Sci., Part A: Poly. Chem. 31, p. 983 (1993)
4 *Komarnemi, S., Parker, J. C., Wollenberger H.:* Mater. Res. Soc. Symp. Proc. (1997), Boston, MA, USA, Dec. 2–5, p. 558 (1997)
5 *Yang, F., Ou, Y., Yu, Z.:* J. Appl. Poly. Sci. 69, p. 355 (1998)
6 *Noh, M. W., Lee, D. C.:* Polym. Bull. 42, p. 619 (1999)
7 *Liu, Z., Qi, Zhu, X.:* J. Appl. Poly. Sci. 71, p. 1133 (1999)
8 *Zilg, C., Thomann, R., Finter, J., Mülhaupt, R.:* Macromol. Mater. Eng. 280(81), p. 41 (2000).
9 *Fu, X. Qutubuddin, S.:* Polymer 42, p. 807 (2001)
10 *Kim, S. W., Jo, W. H., Lee, M. S., Ko, M. B., Jho, J. Y.:* Polymer 42, p. 9837 (2001)
11 *Dennis, H. R., Hunter, D. L., Chang, D., Kim, S., White, J. L., Cho, J. W., Paul, D. R.:* Polymer 42, p. 9512 (2001)
12 *Fornes, T. D., Yoon, P. J., Keskkula, H., Paul, D. R.:* Polymer 42, p. 9929 (2001)
13 *Utracki, L. A., Kamal, M. R.:* Arabian J. Sci. Eng. 25, p. 43 (2002)
14 *Burnside, S. D., Giannelis, E. P.:* Chem. Mater. 7, p. 1597 (1995)
15 *Giannelis, E. P.:* Adv. Mater. 8, p. 29 (1996)
16 *Giannelis, E. P.:* Appl. Organometal. Chem. 12, p. 675 (1998)
17 *Usuki, A., Kojima, Y., Kawasumi, M., Okada, A., Fukushima, Y., Kurauchi, T., Kamigaito, O.:* J. Mater. Res. 8, p. 1179 (1993)
18 *Giannelis, E. P., Krishnamoorti, R., Manias, E.:* Adv. Polym. Sci., 138, p. 107 (1999)
19 *Gilman, J. W., Jackson, C. L., Morgan, A. B., Harris, R. H.:* Chem. Mater. 24, p. 1866 (2000)
20 *Bharadwaj R. K.:* Macromolecules 34, p. 9189 (2001)
21 *Vaia, R. A., Teukolsy, R. K., Giannelis, E. P.:* Chem. Mater. 6, p. 1017 (1994)
22 *Vaia, R. A., Price, G., Ruth, P. N., Nguyen, H. T., Lichtenhan, J.:* Appl. Clay Sci. 15, p. 67 (1999)
23 *Vaia, R. A., Ishii, H., Giannelis, E. P.:* Chem. Mater. 5, p. 1694 (1993)
24 *Okada, A., Usuki, A., Kurauchi, T., Kamigaito, O.:* American Chemical Society, 55–65 (1995)
25 *Manias, E., Strawhecker, K., Touny, A., Wu, L., Kuppa, V.:* Origins of the Materials Properties Enhancements in Polymer/Clay Nanocomposites, http://zeus.plmsc.psu.edu/nano.html
26 *Reichert, P., Nitz, H., Klinke, S., Brandsch, R., Thomann, R., Mülhaupt, R.:* Macromol. Mater. Eng. 278, p. 8 (2000)
27 *Tanoue, S., Utracki, L. A., Garcia–Rejon, A., Tatibouët, J., Cole, K. C., Kamal, M. R.:* Polym. Eng. Sci. 44, p. 1046 (2004)
28 *Tadmor, Z.* in: Integration of Fundamental Polymer Science and Technology. *Kleinjes, L. A., Lemstra, P. J.* (Eds.), Elsevier, Amsterdam (1986)
29 *Rauwendaal, C., Osswald, T., Gramann, P., Davis, B.:* Intern. Polym. Process. 1, p. 28 (1999)
30 *Vaia, R. A., Giannelis, E. P.:* Macromolecules 30, p. 8000 (1997)
31 *Yoon, J. T., Jo, W. H., Lee, M. S., Ko, M. B.:* Polymer 42, p. 329 (2001)
32 *Lebaron, P. C., Wang, Z., Pinnavaia, T. J.:* Appl. Clay Sci. 15, p. 11 (1999)
33 *Choi, H. J., Kim, S. G., Hyon, Y. H., Jhon, M. S.:* Macromol. Rapid. Commun. 22, p. 320 (2001)
34 *Cho, H. W., Paul, D. R.:* Polymer 42 (3), p. 1083 (2001)
35 *Hoffmann, B., Dietrich, C., Thomann, R., Friedrich, C., Mülhaupt, R.:* Macromol. Rapid Commun. 21, p. 57 (2000)
36 *Lee, M. S., Ha, M. G.:* Korea Polym. J. 7 (5), p. 310 (1999)
37 *Xie, W., Gao, Z., Liu, K., Pan, W. P., Vaia, R., Hunter, D., Singh, A.:* Thermochim. Acta 367–368, p. 339 (2001)
38 *Zhu, J., Morgan, A. B., Lamelas, F. J., Wilkie, C. A.:* Chem. Mater. 13, p. 3774 (2001)

Acknowledgments

The assistance of Dr. Kenneth Cole, National Research Council of Canada, in obtaining and interpreting the FTIR spectra is gratefully acknowledged. Financial support was received for the Natural Sciences and Engineering Research Council of Canada.

Date received: February 20, 2005
Date accepted: July 25, 2005